Mechanism and Machine Theory 92 (2015) 314–329

Contents lists available at ScienceDirect

Mechanism and Machine Theory

journal homepage: www.elsevier.com/locate/mechmt

An adjustable gravity-balancing mechanism using planar extension and compression springs

Zong-Wei Yang, Chao-Chieh Lan *

Department of Mechanical Engineering, National Cheng Kung University, No. 1, University Road, Tainan City 701, Taiwan, ROC

ARTICLE INFO

Article history:
Received 5 June 2014
Received in revised form 5 May 2015
Accepted 11 May 2015
Available online 20 June 2015

Keywords:
Gravity balancing mechanisms
Nonlinear springs
Compliant mechanisms

ABSTRACT

Passively compensating a payload weight requires a mechanism that can generate a nonlinear torque curve. Existing gravity-balancing mechanisms (GBMs) rely on linear or torsional springs with various principles to generate the required torque profile. This paper presents the design of a novel GBM whose balancing capability can be adjusted. The idea is to employ two linear springs, one extension spring and one compression spring, to synthesize the required nonlinear torque curve. The springs are concentrated on the base joint to reduce the overall size. An optimization formulation is given to maximize the weight compensation capability. The effects of various parameters on the achievable weight are discussed. Low-volume planar springs are specifically designed to serve as the linear springs so that large stiffness can be generated in a limited space. By preloading the springs, the GBM can easily adjust its torque curve to match different payloads. An illustrative prototype is given with experiment verifications to demonstrate the claimed merits of the proposed GBM.

1. Introduction

A robotic manipulator relies on actuators to support and transport its moving links and external payload. Each actuator needs to be large enough to provide sufficient torque. When the actuators are embedded in a manipulator, the heavy actuators would make the manipulator bulky and energy-inefficient. Because the total weight of the payload and the moving links are often known in advanced, gravity-balancing mechanisms have been proposed for the weight compensation. A gravity-balancing mechanism (GBM) can maintain the total potential energy of a manipulator constant by passively transferring the energy in or out of an energy storage element. Statically, no force is required to produce motion. The manipulator shows a zero-stiffness property. Because minimum torque is required for the actuators, the manipulator requires only small actuators and becomes lighter.

Existing weight compensation approaches are mostly based on counterweights [1,2] and spring mechanisms [3–9]. Fig. 1(a) shows the schematic of a counterweighted manipulator. Using a counterweight is simple and can balance all positions. It has been applied for many industrial manipulators. Because a counterweight is usually heavier than the payload, it is not suitable for applications where weight is a concern. Spring mechanisms are more attractive because springs can be assumed weightless. Fig. 1(b)–(e) shows four different spring mechanisms. Each creates a moment arm variation in order to produce the nonlinear torque curve required for gravity balance. The type in Fig. 1(b) is the simplest (e.g., Ref. [4]). To avoid interference with other components, the protruded spring over the links should be avoided. This can be resolved by embedding the spring on the link, as shown in Fig. 1(c). This type requires a large hollow link to store the spring (e.g., Refs. [5,6]). Another way to hide the spring is to use a parallelogram (e.g., Ref. [7]), as shown in Fig. 1(d). This type can be extended to compensate manipulators with multiple degrees-of-freedom. However, the parallelogram

* Corresponding author. Tel.: +886 6 2757575x62274; fax: +886 6 2352973.
E-mail addresses: blue90126@gmail.com (Z.-W. Yang), cclan@mail.ncku.edu.tw (C.-C. Lan).

http://dx.doi.org/10.1016/j.mechmachtheory.2015.05.006
0094-114X/

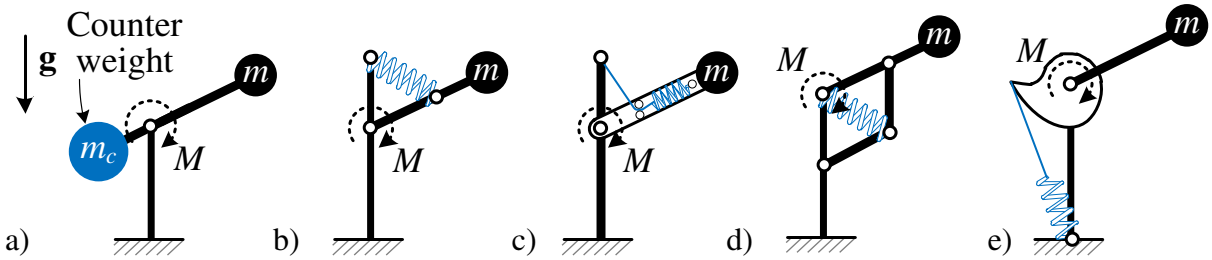

Fig. 1. Different types of GBMs: (a) Counterweight; (b) External spring; (c) Internal spring; (d) Parallelogram; (e) Cable-cam.

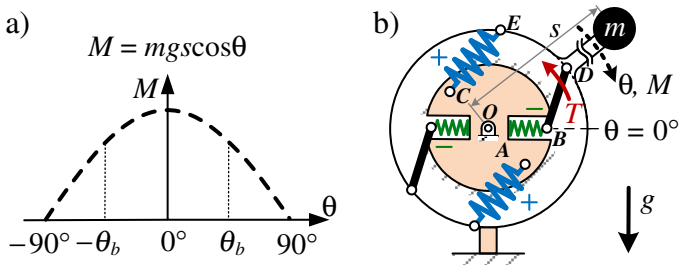

Fig. 2. (a) M–θ curve of a manipulator; (b) Schematic of the proposed GBM.

introduces non-negligible link weight and needs to be large enough to place the spring diagonally. Using a cam can also produce a nonlinear torque curve (e.g., Ref. [8]). The springs used in GBMs are mostly assumed to have zero free length. Because a spring practically has a nonzero free length, wires and pulleys are required to relocate and reorient the springs in order to emulate the condition of zero free length. The additional components would increase the mechanism size.

A major challenge of GBMs is the required complexity to adapt the mechanism to compensate different payload weight. For the spring mechanisms in Fig. 1(b)–(e), these often require adjustment of the spring attachment point or spring stiffness. Adjusting the attachment point is not convenient because it requires extra work in practice. Adjusting the spring stiffness could be achieved via changing the active length of the spring [9]. Because the spring is usually very long, a considerable length change is required in order to significantly change the load capacity. The adjustment mechanism hence becomes larger and occupies a big portion of the GBM. When the spring is loaded, a substantial force is required to change the spring length. An energy-free adjustment method [10] has been proposed to minimize the adjustment force.

In addition to robotic manipulators, GBMs have been applied to design desktop lamps [11], motion stabilizers [12], and support devices [13,14] for disabled people. Recently, they are extended to design passive exoskeletons [15,16] wore on human limbs. When a gravity-balancing exoskeleton is used for limb rehabilitation, the limb weight can be supported such that the weakened limb can move with minimal muscular force. When used for motion assist, the exoskeleton can assist human in strenuous activities. To ensure sufficient wearability, mobility, and safety, an exoskeleton must be compact and free of interference with human motion. However, reducing the size and weight of a gravity-balancing exoskeleton without compromising its compensation capability remains difficult. Most GBMs have protruded components that may collide with human body during operation.

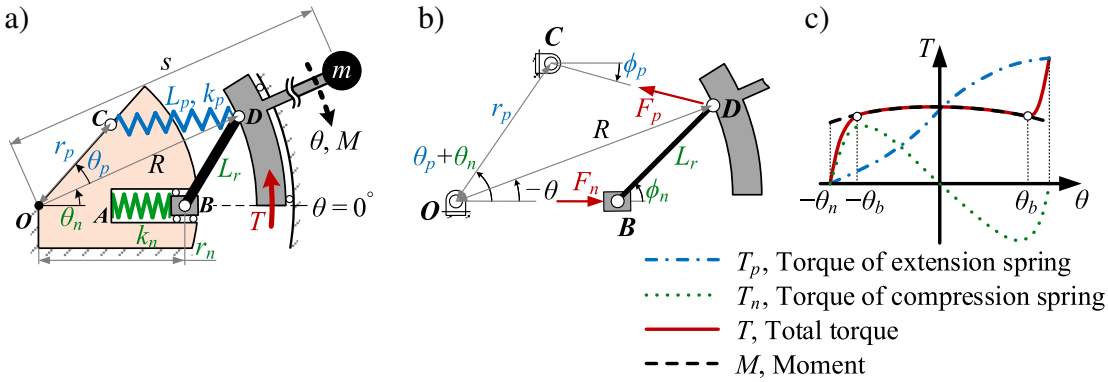

Fig. 3. (a) Design model of the GBM; (b) Free-body diagram of the rigid link and outer rim; (c) Torque and moment curves.

Table 1
GBM design parameters.

Outer rim radius, R	75 mm
Arm length, s	150 mm
Balancing range, $[-\theta_b\ \theta_b]$	$[-26°\ 26°]$
Compression spring stiffness, k_n	5 N/mm
Elongation ratio, ε	0.25

This paper proposes a new GBM with adjustable balancing capacity. Different from traditional balancing methods that seek a constant potential energy, the proposed idea is to employ two linear springs, one extension spring and one compression spring, to synthesize the required nonlinear torque curves for weight compensation. In what follows, the model and parametric optimization of the GBM is formulated in Section 2. Section 3 proposes an adjustment method to compensate different payloads. To minimize the mechanism size, a special planar spring design scheme is presented in Section 4. Finally in Section 5, a prototype is presented with experiment verification.

2. Design of the gravity-balancing mechanism

2.1. Design concept

Considering one degree-of-freedom manipulators as those shown in Fig. 1, the moment M produced by the payload weight on the base joint is illustrated in Fig. 2(a). The sinusoidal moment curve has its peak at $\theta = 0°$ and gradually reduces to zero at $\theta = -90°$ and 90°. The goal of a GBM is to produce a reaction torque curve having the same magnitude as the moment curve in order to completely balance the payload weight. For a reasonable balancing range from $-\theta_b$ to θ_b, the moment curve is nonlinear and symmetric about the axis of $\theta = 0°$. A typical torsional spring can only produce a linear torque curve and hence is not suitable. Because the moment curve in Fig. 2(a) has a positive stiffness segment before $\theta = 0°$ and a negative stiffness segment after $\theta = 0°$, a GBM must be able to exhibit such stiffness variation. To meet this requirement, we proposed a new GBM as shown in Fig. 2(b). Four springs connect the inner fixed shaft to the outer rim with rotational symmetry. When the outer rim rotates clockwise due to the payload weight, a reaction torque T is generated at the base joint O. To produce the torsional stiffness variation, the springs with mark "+" extend to provide a positive stiffness. The springs with mark "−" inside the slots are compressed through the rotation of the connecting rigid links to provide a negative stiffness. For brevity, they are referred to as the extension and compression springs, respectively. The magnitudes of the positive and negative stiffnesses depend on the spring stiffnesses, link dimension, and initial joint positions. When the positive and negative stiffnesses properly match, the GBM can generate a nonlinear torque curve to cancel with the moment curve shown in Fig. 2(a). We have used similar stiffness-matching principles in our earlier work to design constant-force mechanisms [17] and variable-stiffness mechanisms [18].

2.2. Modeling and optimization of the proposed GBM

Fig. 3(a) shows the design model. The mechanism has a nearly sectorial shape whose size can be described by the radius R. Compared with that in Fig. 2(b), we focus on one pair of extension and compression springs in order to reduce the sector area. Because the two springs act independently to obtain their respective torque curves, their relative position can be arbitrarily selected. The extension spring is thus moved closer to the compression spring such that joints D and E in Fig. 2(b) coincide. Using a single joint (D) to connect the extension spring and rigid link can further reduce the size and assembly complexity. The springs shown in Fig. 3(a) are in their initial undeformed positions. The stiffnesses of the extension and compression springs are denoted as k_p and k_n. Symbols L_p and L_r denote the length of the extension spring and rigid link, respectively. Lengths r_p and r_n define the end positions of the two springs, whereas angles θ_p and θ_n define the initial orientations of the two springs. A payload of mass m is placed along line O–D with a distance s from joint O. The angle of rotation of the payload is denoted as θ. Initially, θ is equal to $-\theta_n$.

Table 2
Optimized design variables of the GBM.

$k_p = 13.04$ N/mm	$R_{sq} = 0.95$
$r_p = 16.34$ mm	$m = 1.30$ kg
$r_{n0} = 42.75$ mm	
$\theta_p = 45.82°$	
$\theta_n = 33.41°$	

Using the free-body diagram in Fig. 3(b), the reaction torque of the GBM can be derived as a function of θ.

$$T = T_p + T_n \\ \text{where } T_p = -r_p F_p \sin\left(\phi_p - \theta_p - \theta_n\right) \text{ and } T_n = RF_n\left(\tan\phi_n \cos\theta + \sin\theta\right). \tag{1}$$

The symbols T_p and T_n in Eq. (1) represent the reaction torques from the extension and compression springs, respectively. Angles ϕ_p and ϕ_n measure the orientations of the extension spring and rigid link with respect to the horizontal axis, respectively. They can be expressed as

$$\phi_p = \tan^{-1}\left[\frac{-R\sin\theta - r_p \sin\left(\theta_n + \theta_p\right)}{R\cos\theta - r_p\cos\left(\theta_n + \theta_p\right)}\right], \tag{2}$$

$$\phi_n = \tan^{-1}\left(\frac{-R\sin\theta}{R\cos\theta - r_n}\right). \tag{3}$$

Using Δ_p to denote the elongated length of the extension spring and Δ_n to denote the compressed length of the compression spring, the spring forces F_n and F_p can be represented as

$$F_p = k_p\Delta_p \text{ where } \Delta_p = L_p\Big|_{\theta=-\theta_n}^{\theta=\theta}, \tag{4}$$

$$F_n = -k_n\Delta_n \text{ where } \Delta_n = r_n\Big|_{\theta=-\theta_n}^{\theta=\theta}. \tag{5}$$

Based on the geometric relationship of the mechanism, the lengths L_p and r_n in Eqs. (4)–(5) can be obtained using

$$L_p = \left[R^2 + r_p^2 - 2Rr_p\cos\left(\theta_p + \theta_n + \theta\right)\right]^{1/2}, \tag{6}$$

$$r_n = R\cos\theta - \left(L_r^2 - R^2\sin^2\theta\right)^{1/2} \text{ where } L_r = \left(r_{n0}^2 - 2r_{n0}R\cos\theta_n + R^2\right)^{1/2}. \tag{7}$$

By setting $\theta = -\theta_n$, the initial spring length L_{p0} can be obtained from Eq. (6). In Eq. (7), r_{n0} represents the initial length of r_n when $\theta = -\theta_n$. Using Eqs. (1)–(7), the reaction torque curves can be obtained. Fig. 3(c) illustrates the torque curves of the GBM. Through rotation of the outer rim, the force of the extension spring is transformed to produce a nearly linear torque curve (dashed–dotted line) whose positive stiffness is slightly bigger for $\theta < 0°$ and slightly smaller for $\theta > 0°$. This stiffness variation is due to the nonlinear relationship between T_p and θ in Eq. (1). By rotating the rigid link, the force of the compression spring is transformed to produce a bistable torque curve (dotted line) with a large negative stiffness segment in the balancing range. The sum of the two torque curves is represented as a solid line that is expected to match with the moment curve (dashed line) in the balancing range. When well-balanced, the magnitudes of positive and negative stiffnesses will be almost equal at $\theta = 0°$. Using two springs is the fundamental requirement of the proposed GBM. While it is possible to use a linear torsional spring mounted at joint O to replace the extension spring, its linear torque curve would cause much larger balancing error than using the extension spring.

For a given arm length s, size R, and balancing range θ_b, the payload that can be supported by the GBM depends on the initial locations and stiffnesses of the two springs. To obtain the best balancing capability, a numerical optimization is proposed as in Eqs. (8)–(9). The objective is to maximize the mass of the payload (m) to be balanced. The design variables are k_p, k_n, r_p, r_{n0}, θ_p, and θ_n that determine the shape of the torque curves.

There are five constraints in Eq. (9) to ensure convergence and that the converged design variables render a feasible GBM. Constraints g_1 and g_2 are used to prevent the spring parameters from being negative. To make sure that the extension and compression springs provide the expected torque curves as shown in Fig. 3(c), constraint g_3 confines the values of θ_p and θ_n to be within 0° and 90°. A practical spring of a finite length has a limited deformation length. Constraint g_4 is used to prevent the elongation of the extension spring from exceeding a prescribed ratio ε. The compression spring does not require such constraint because its natural length can always be extended to reduce the deformation ratio to a proper value. The natural length extension can be achieved by moving point A to the left, if interference is not a problem. Finally, constraint g_5 enforces the reaction torque T to match with the moment M in the balancing range. We use the coefficient of determination R_{sq} to indicate how well the torque curve matches the moment curve. The definition of

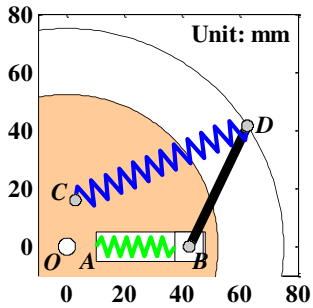

Fig. 4. Mechanism configuration.

R_{sq} is expressed in Eq. (10). The closer the value of R_{sq} is to one, the better the torque curve fits the moment curve. In our design, the value of R_{sq} needs to be at least 0.95.

$$\text{Maximize } m \tag{8}$$

$$\text{Subject to } \begin{cases} g_1: & r_{n0}, r_p \geq 0 \text{ mm}; \\ g_2: & k_p, k_n \geq 0 \text{ N/mm}; \\ g_3: & 0^\circ \leq \theta_n, \theta_p \leq 90^\circ; \\ g_4: & \Delta_p / L_{p0} \leq \varepsilon; \\ g_5: & R_{sq} \geq 0.95. \end{cases} \tag{9}$$

$$R_{sq} = 1 - \Sigma(T-M)^2 / \Sigma(T-\overline{T})^2, \text{ where } \overline{T} \text{ is the average of } T \text{ within } -\theta_b \text{ and } \theta_b. \tag{10}$$

2.3. Results and discussions

Table 1 lists the design parameters. The outer rim radius and arm length were assumed reasonable values. We chose $\theta_b = 26°$ in order to have a large balancing range. For Eqs. (8)–(9) to be a valid optimization, either one of the two spring stiffnesses must be pre-specified. As an illustration, we selected the stiffness of the compression spring to be 5 N/mm. The elongation ratio was set as 0.25. Using `fmincon()` in MATLAB as the optimization solver, the optimal design variables could be computed, as listed in Table 2. The value of k_p was almost three times greater than the value of k_n. The values of m and R_{sq} were also given, where R_{sq} reached its lower limit. Fig. 4 shows the optimal initial configuration of the GBM. The corresponding T–θ, T_p–θ, and T_n–θ curves were plotted in Fig. 5, along with the M–θ curve. The T–θ and M–θ curves matched well in the balancing range, indicating that R_{sq} of 0.95 was high enough to ensure proper balancing. The largest discrepancy occurred near the two boundaries of the balancing range. If slight unbalance can be tolerated, a smaller R_{sq} limit (say, 0.90) can be assigned in order to increase the payload mass.

To increase the compensation capability of the proposed GBM, we can use more pairs of extension and compression springs (e.g., two pairs as shown in Fig. 2(b)) to increase the magnitude of the torque curves. However, using more pairs would increase the GBM size and complexity. Because the achievable payload mass is proportional to the spring stiffness, a simpler way is to increase the stiffnesses of the two springs without altering the stiffness ratio. If both k_p and k_n are increased by a factor α, the torque is also multiplied by α. To achieve the same deformation ratio, an increase of spring stiffness would increase the spring size as well. The original mechanism cannot accommodate larger springs. In this case, the mechanism dimension needs to be scaled up. This is achieved by multiplying the length parameters (R, r_p, and r_{n0}) by a factor β without changing the angle parameters (θ_p and θ_n). When the dimension is multiplied by β, the torque is multiplied by the square of β. The following formula can be used to calculate the new torque magnitude when the mechanism dimension and spring stiffness are scaled.

$$T_2 = \alpha\beta^2 T_1 \tag{11}$$

where T_1 and T_2 are the original and new torques, respectively. For the same arm length s, the achievable mass is also multiplied by $\alpha\beta^2$. The scaled mechanism would have the same R_{sq} and ε.

2.4. Investigation on the design parameters

In Table 1, the values of ε and θ_b were illustrative. Sections 2.4.1–2.4.2 respectively studied the effects of the two design parameters on the balancing performance. For each parameter, five different values were tested while the other design

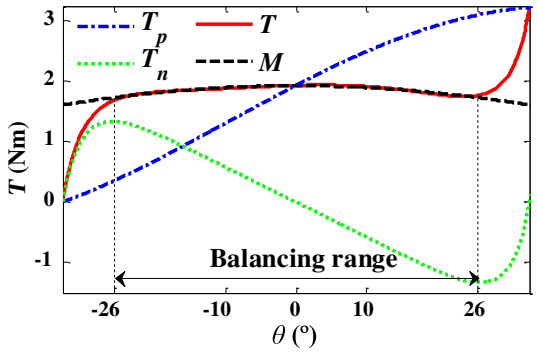

Fig. 5. Optimized torque curves.

parameters were the same as those in Table 1. The same optimization was performed for each case. The optimized results of ε and θ_b were compared in Tables 3 and 4, respectively. For all optimization cases, the coefficients of determination reached 0.95.

2.4.1. Effect of elongation ratio

For the optimization result in Section 2.3, constraint g_4 became active. This indicates that a larger ε can increase the payload mass. Five different values of ε were compared: 0.15, 0.20, 0.25, 0.30, and 0.35. Fig. 6 shows the mechanism configurations of using $\varepsilon = 0.20$ and 0.30. Table 3 lists the optimization results. For each case, the extension spring reached its prescribed elongation ratio. Although a larger ε could increase the spring force, this was counteracted by the decrease of the extension spring stiffness. Hence, the achievable payload mass only marginally increased. Because the extension spring stiffness significantly depends on the elongation ratio, the value of ε can be used to determine an appropriate stiffness ratio k_p/k_n. For size considerations, a spring with a larger elongation ratio requires a larger space. If the increase of m is small compared with the increase of ε, a smaller elongation ratio is more preferable in order to reduce the mechanism size. When the elongation ratio is too small, it can be observed from Fig. 6 that joint C would move too close to joint O and cause possible interference. Thus a reasonable elongation ratio should be assigned.

2.4.2. Effect of the balancing range

To obtain a larger balancing range, the value of θ_b should be increased. Five different values of θ_b were tested: 16°, 21°, 26°, 31°, and 36°. Fig. 7 shows the torque curves of using $\theta_b = 31°$ and 36°. Both torque curves matched the corresponding moment curves very well. Fig. 8 shows the mechanism configurations of using $\theta_b = 31°$ and 36°. Table 4 compares the optimized results. To obtain a larger balancing range, the negative-stiffness range of the bistable torque curve should increase. As shown in Fig. 8, this required a longer L_r. For the same stiffness k_n of 5 N/mm, the magnitude of the negative stiffness in Fig. 7 would decrease. The magnitude of the positive

Table 3
Comparison of using different values of ε.

ε	k_p (N/mm)	r_p (mm)	r_{n0} (mm)	θ_p (°)	θ_n (°)	m (kg)
0.15	31.19	10.41	42.36	49.96	33.46	1.27
0.20	18.90	13.48	42.58	47.81	33.42	1.29
0.25	13.04	16.34	42.75	45.82	33.41	1.30
0.30	9.76	19.03	42.97	43.93	33.36	1.32
0.35	7.74	21.55	43.20	42.21	33.29	1.34

Table 4
Comparison of using different values of θ_b.

θ_b	k_p (N/mm)	r_p (mm)	r_{n0} (mm)	θ_p (°)	θ_n (°)	m (kg)
16	14.85	23.89	59.60	50.36	22.22	2.18
21	15.11	19.33	51.72	48.64	27.89	1.79
26	13.04	16.34	42.75	45.82	33.41	1.30
31	9.33	14.28	32.96	42.46	38.72	0.81
36	5.05	12.79	22.51	38.81	43.85	0.39

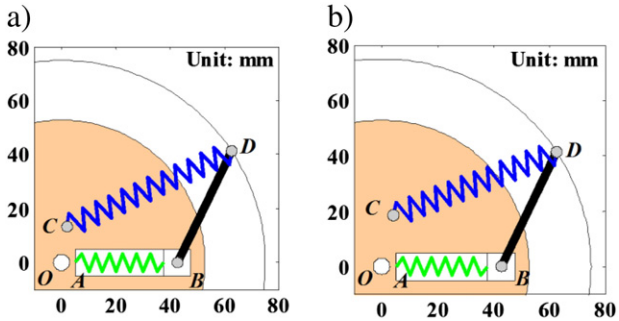

Fig. 6. Mechanism configurations: (a) $\varepsilon = 0.20$; (b) $\varepsilon = 0.30$.

stiffness would decrease as well in order to match with the negative stiffness. The small stiffness values resulted in smaller payload mass. The achievable payload for $\theta_b = 31°$ and 36° were 0.81 and 0.39 kg, respectively. To increase the payload mass for a large balancing range, the stiffness of the compression spring should be amplified.

2.5. Asymmetric balancing range

Because θ is initially equal to $-\theta_n$, the balancing range needs to be symmetric about $\theta = 0°$. When this relationship is relaxed, the GBM can be extended to scenarios where the balancing range is not symmetric about $\theta = 0°$. As an illustration, two optimization cases were provided. They used the same optimization formulation as in Eqs. (8)–(9) and the same design parameters as in Table 1 except that the balancing ranges were different. Fig. 9 shows the torque curves of the first optimization. The balancing range was from $-3°$ to 49°. A payload of 2.57 kg could be balanced. Fig. 10 shows the torque curves of the second optimization. The balancing range was from $-49°$ to 3°. A payload of 4.61 kg could be balanced. Table 5 shows the optimized design variables of both cases. For both cases, the values of R_{sq} reached the lower limit.

3. Adjustment for different payload mass

Eq. (11) was given in Section 2.3 to facilitate the design of GBMs to balance different payloads. In practice, the payload mass may deviate from its original value in different scenarios. The proposed GBM can be adjusted on-line to balance different payloads by simply preloading the extension spring. Fig. 11(a) shows the diagram of spring preload. A preload screw is inserted between joint C and one end of the extension spring. To make sure that the spring elongation is always along line C–D, the other end of the extension spring is attached to a slider. The spring, slider, and screw are all located inside a linear guide. By turning the screw, a displacement preload δ_p for the spring can be created. Corresponding to the preload, the spring force F_p in Eq. (4) should be rewritten as

$$F_p = k_p\left(\Delta_p + \delta_p\right). \tag{12}$$

According to Eq. (1), this displacement preload will increase the magnitude of the total torque curve by the amount $-r_p k_p \delta_p \sin(\phi_p - \theta_p - \theta_n)$. This amount involves ϕ_p and hence the magnitude of increase depends on θ. Fig. 11(b) shows the schematic of the torque

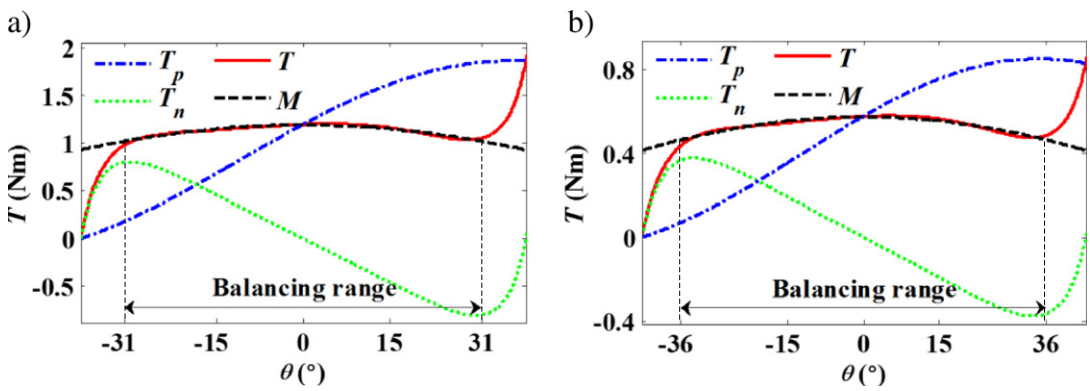

Fig. 7. Torque curves: (a) $\theta_b = 31°$; (b) $\theta_b = 36°$.

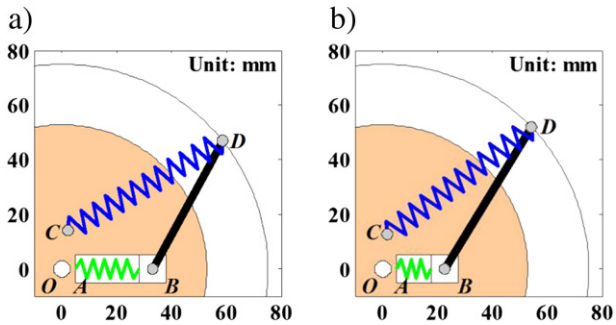

Fig. 8. Mechanism configurations: (a) $\theta_b = 31°$; (b) $\theta_b = 36°$.

curves with preloads. Positive and negative preloads would increase and decrease the curve magnitude, respectively. The amount of torque curve change is proportional to the product of the extension spring stiffness and preload. A changed torque curve can be used to match with the moment curve of a different payload. By ensuring that the torque and moment are equal at $\theta = 0°$, the following formula is derived to obtain the required preload for a new payload mass m.

$$\delta_p = \frac{-mgs}{r_p k_p \sin\left[\phi_p(0^\circ) - \theta_p - \theta_n\right]} - L_p\Big|_{\theta=-\theta_n}^{\theta=0^\circ} \tag{13}$$

where $\phi_p(0^\circ)$ denotes ϕ_p evaluated at $\theta = 0°$. As an illustration, the torque curve in Fig. 5 could be changed using $\delta_p = -0.08L_{p0}$, 0, and $0.08L_{p0}$. Fig. 12 shows the changed torque curves. The curve of $\delta_p = 0.08L_{p0}$ could balance a payload mass of 2.05 kg, which was nearly 1.5 times greater than the original mass. The curve of $\delta_p = -0.08L_{p0}$ could balance a payload mass of 0.55 kg, which

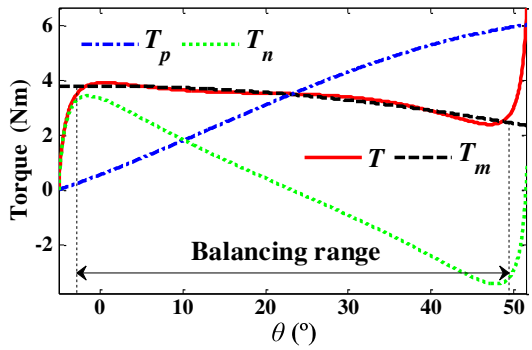

Fig. 9. Optimized torque curves (balancing range from −3° to 49°).

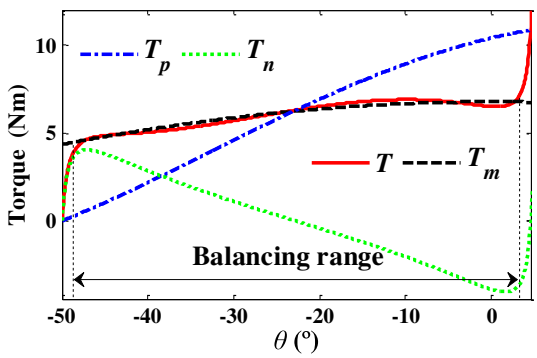

Fig. 10. Optimized torque curves (balancing range from −49° to 3°).

Table 5
Optimized design variables of using different balancing range.

Balancing range	k_p (N/mm)	r_p (mm)	r_{n0} (mm)	θ_p (°)	θ_n (°)	m (kg)
−3° to 49°	22.80	17.92	57.74	51.51	28.22	2.57
−49° to 3°	40.88	18.26	60.19	52.65	27.29	4.61

was nearly 40% of the original mass. Thus a slight preload (roughly ±5 mm) can offer a significant payload adjustment. The moment curves of $m = 2.05$ and 0.55 kg were also plotted in Fig. 12. The torque curves matched the moment curves well. The maximum difference was 0.05 Nm. For the curves of $\delta_p = -0.08L_{p0}$ and $0.08L_{p0}$, the stiffnesses in the balancing range slightly changed with respect to the curve of $\delta_p = 0$. These stiffness changes were consistent with the stiffness changes of the corresponding moment curves. To adjust the GBM for a larger range of payload mass deviation, a larger magnitude of δ_p should be used.

4. Design of the linear springs

4.1. Spring shape to avoid interference

Existing GBMs mostly use coil springs to store and release the potential energy. For the same deformation ratio, the stiffness of a coil spring increases with its size. For our GBM, the space to install the springs is relatively small considering their large stiffnesses and elongation lengths. Commercially available coil springs can barely fit. Even if coil springs are used, they would interfere with each other because the springs are made very close to each other. Fig. 13(a) shows the schematic of the GBM at $\theta = 26°$, where the extension spring interferes with the compression spring. To achieve the required stiffness of 13.04 N/mm, the extension spring in Fig. 13(a) needs to have a diameter of at least 20 mm. The large diameter would result in a large interference range from $\theta = -5°$ to 26°, which is more than half of the balancing range. Although the two springs can be arranged in different planes, the lateral size of the GBM would adversely increase. The best way is to design the two springs using different geometries such that they do not overlap in the same plane. Fig. 13(b) shows the schematic of the proposed design, where both springs have inverted U-shaped planar structures instead of coils. In Fig. 13(b), the inverted U-shape of the extension spring is larger than that of the compression spring. The spring shapes make it possible for the two springs to move in the same plane without overlap. At the end of rotation, the compression spring is totally inside the extension spring.

Different inverted U-shapes are possible. As long as the spring is symmetric about the midline between its two ends, the spring stiffness will be a constant. The design principle is to find a spring shape that has a minimum size while the desired stiffness and deformation can be achieved without exceeding a specified stress limit. To simplify the design, two shapes for the extension spring are proposed. The simplest shape, denoted as Type I, is shown in Fig. 14(a). Type I mainly consists of two side beams and one top beam connected at right angles. As an illustration, the top spring is given a length of $1.4L_{p0}$ (L_{p0} is the initial distance between joints C and D) in order to achieve the required stiffness and elongation length. Using a larger length for the top beam is possible but the spring would be larger. This would increase the overall size of the GBM. The two ends of the spring are connected to the top of two O-shaped rings. The O-shaped rings are for mounting pins to rotate at joints C and D. Fig. 14(b) shows a more complicated shape, denoted as Type II. Part of each side beam is replaced by a series of connected short beams. The six short beams, each with a length of L_1, are equally spaced. Without causing interference, the purpose of the short beams is to increase the effective length of the side beams in the same space. Hence the desired stiffness (13.04 N/mm) and elongation ratio (0.25) can be achieved using a smaller spring height H. There is a distance L_2 from the lowest short beam to the O-shaped ring to avoid spring self-interference during deformation. The top beam remains straight in order not to interfere with the compression spring.

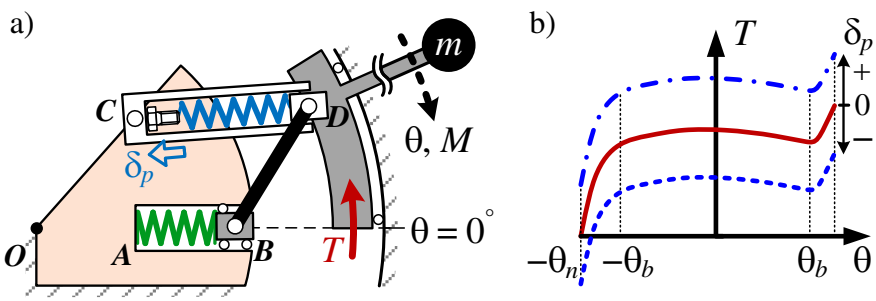

Fig. 11. (a) Schematic of spring preload; (b) Torque curves of using preloaded extension spring.

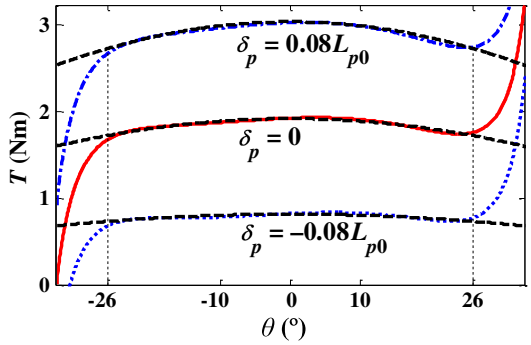

Fig. 12. Torque curves with $\delta_p = -0.08L_{p0}$, 0, and $0.08L_{p0}$.

4.2. Optimization of spring height

Table 6 lists the design parameters for the extension spring. The required parameters were from those obtained in Sections 2.2–2.3. The value of Δ_p included the preload of $0.08L_{p0}$ in order to provide payload adjustments. The given parameters determined the detailed dimensions of the extension spring. Based on the parameters in Table 6, the height H and in-plane thickness w could be chosen to achieve the required stiffness and elongation length. To minimize the spring size without causing material failure, a numerical optimization was performed to find the smallest H while the maximum stress σ_m of the material was within a specific limit σ_a. The optimization was formulated as follows.

$$\text{Minimize } H \quad \text{Subject to} \begin{cases} \sigma_m \le \sigma_a; \\ k_p = 13.0392 \ \text{N/mm}; \\ \Delta_p = 21.3427 \ \text{mm}. \end{cases} \tag{14}$$

In this paper, we used plastic mold steel (S-STAR) as the material for the springs to obtain large stiffness. A stress limit of 1 GPa was assigned to this material. Using the GMSM [19,20] as the computational tool to facilitate the deformation analysis, the minimal spring height was found. Table 7 compares the optimized parameters of Types I and II. Type I had a much bigger H compared with Type II. The in-plane thickness of Type I was also larger than that of Type II. This is because the two side beams of Type I are straight with total length smaller than that of Type II. Hence, they need to be longer and thicker in order to achieve the required stiffness while limiting the maximum stress to be smaller than 1 GPa. To reduce the spring size, Type II was chosen for the extension spring.

Similarly for the compression spring, Fig. 15 shows two types of shape design schemes. The initial length between joints A and B is denoted as L_{n0}. Different from the extension spring whose initial length L_{p0} needs to meet the design requirement, the length L_{n0} can be arbitrary selected. Type III has an inverted U-shape, whereas Type IV has a series of short beams forming the top beam. Similar to those of Type II, the 12 short beams, each having length of L_3, are equally spaced. The two side beams remain straight in order to avoid interference with neighboring components. Based on the parameters given in Table 8 and using the same optimization formulation as that for the extension spring, the minimum height of the compression spring

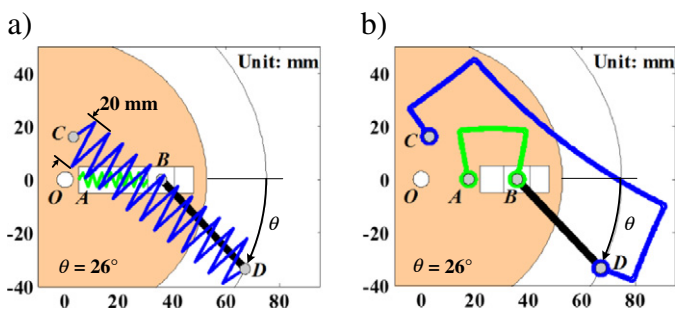

Fig. 13. (a) Schematic of spring interference; (b) Inverted U-shaped springs to avoid interference.

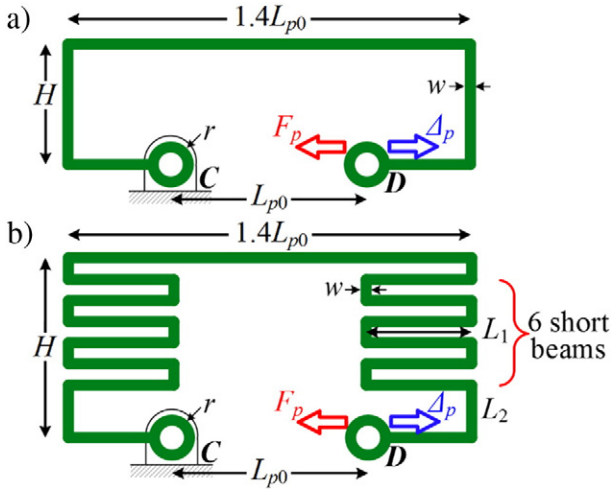

Fig. 14. Two types of shape for the extension spring: (a) Type I; (b) Type II.

could be found. The results were again compared in Table 7. Similar to that of the extension spring, Type IV had a much smaller height than Type III. Hence it was chosen for the compression spring. For both the extension and compression springs, the use of multiple short beams can reduce the height by nearly half. The height of the springs can be made even smaller by increasing the length of the short beams. However, the width of the extension spring would increase as well.

Fig. 16(a–b) shows the original shapes of the two optimized springs. The deformed shapes of $\Delta_p = 21.34$ mm and $\Delta_n = 13.57$ mm were also plotted. The relative position of the two springs was shown in Fig. 16(c). As can be seen, there was no interference of the two springs. Based on the optimized spring shapes, the extension and compression springs were fabricated using wire electrical-discharge machining. Fig. 17 shows the fabricated springs. Loading experiments were conducted to verify the stiffness of the optimized springs. Fig. 18(a–b) shows the force-to-displacement curves of the extension and compression springs, respectively. Both springs had very linear force curves. The stiffnesses of the extension and compression springs were 12.42 and 5.17 N/mm, respectively. They almost matched the require stiffnesses of 13.04 N/mm and 5 N/mm. For each spring, the maximum stress increased linearly with the displacement. The maximum stress occurred at the two ends of the top beam for the extension spring. For the compression spring, the maximum stress occurred at the midpoint of the top beam.

The shapes of the springs are not limited to those presented in Figs. 14–15. As long as a constant stiffness can be achieved for a spring shape (e.g., by ensuring linearity in the optimization), it can be used as the extension or compression spring. The key is how to achieve the required stiffness and elongation length with a minimum spring size. To avoid interference and overstress, the spring usually requires a winded shape similar to those in Figs. 14–15.

Table 6
Design parameters of the extension spring (Types I and II).

Required	Given
$L_{p0} = 64.68$ mm	Out-of-plane thickness, $t = 10$ mm
$k_p = 13.04$ N/mm	O-ring radius, $r = 3.5$ mm
$\Delta_p = 21.34$ mm	Short beam length, $L_1 = 15.5$ mm
	Clearance, $L_2 = 9$ mm

Table 7
Comparison of different spring shapes.

	Type I	Type II	Type III	Type IV
w (mm)	3.10	2.28	1.23	0.83
H (mm)	59.34	29.14	36.67	15.37

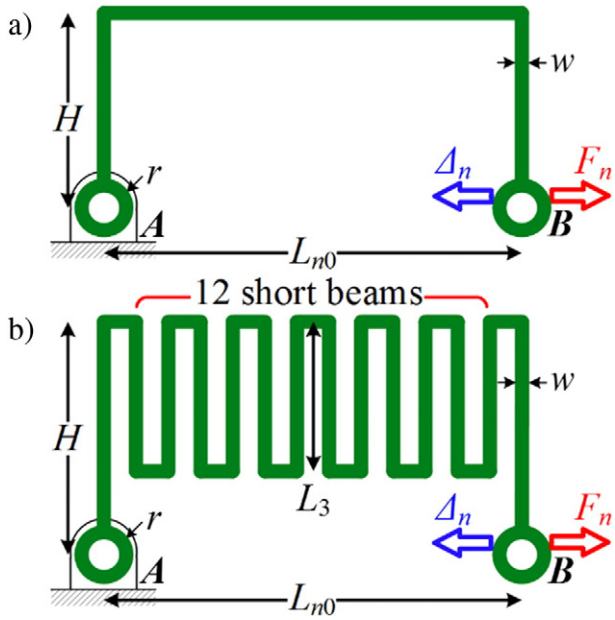

Fig. 15. Two types of shape for the compression spring: (a) Type III; (b) Type IV.

5. Prototype and experiment

5.1. Prototype and experimental setup

Based on the designs in Sections 2–4, a prototype of the GBM was presented. The mechanism dimensions were from those listed in Tables 1 and 2. The extension and compression springs were from those presented in Fig. 17. Fig. 19(a) shows the CAD model of the GBM and Fig. 19(b) shows the interior view. The GBM had a size of $104 \times 85 \times 38$ mm^3. The two springs were placed in the middle layer while the two outside layers were for placing the rigid links, preload screws, and linear guides. The whole mechanism was symmetric about the middle layer. The symmetric arrangement could avoid unnecessary forces in the lateral direction. The two preload screws (M3) were on the outside of the mechanism, making it easier to preload the extension spring. The end of the long rod was for mounting a payload.

Fig. 20 shows the fabricated and assembled GBM and Fig. 21 shows the experimental setup. To measure the reaction torque, the mechanism was mounted on a rotary motorized stage that rotated against two stationary force sensors (FUTEK LSB200). The force sensors were placed at $s = 150$ mm. When the motorized stage rotated counterclockwise, the measured normal contact force could be converted to the reaction torque T.

5.2. Results

Experiments of three different preloads were conducted: $\delta_p = 3, 0$, and -3 mm. The three preloads were used to balance payload masses of 1.73, 1.30, and 0.86 kg, respectively. The preloads of the extension spring could be achieved manually using a screwdriver, as shown in Fig. 22. For an M3 screw with a pitch of 0.5 mm, six turns were required to complete the adjustment. Screws of finer pitch could be further used to increase the adjustment resolution. The measured torques curves in the loading direction were shown in

Table 8
Design parameters of the compression spring (Types III and IV).

Required	Given
$k_n = 5$ N/mm $\Delta_n = 13.57$ mm	Out-of-plane thickness, $t = 10$ mm Initial spring length, $L_{n0} = 25$ mm O-ring radius, $r = 3.5$ mm Short beam length, $L_3 = 8.5$ mm

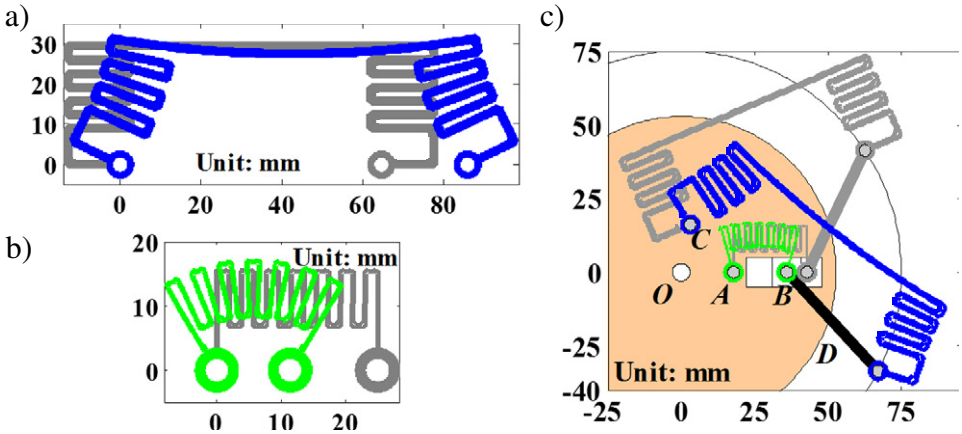

Fig. 16. (a–b) Original and deformed shapes of the extension and compression springs (Types II and IV); (c) Relative position of the two springs when $\theta = -33.41°$ and 26°.

Fig. 17. (a) Extension spring (Type II); (b) Compression spring (Type IV).

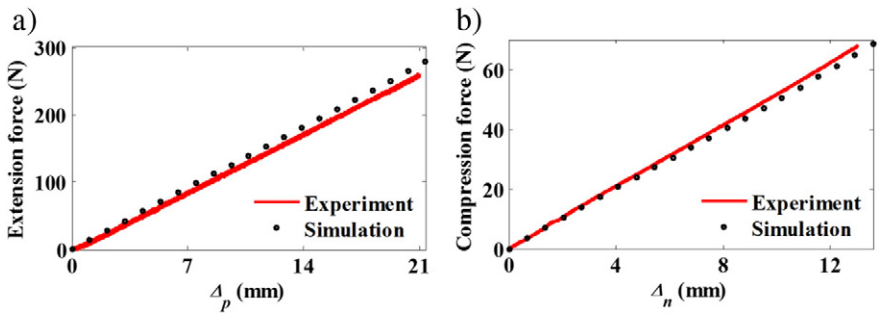

Fig. 18. Experimental force curves: (a) Extension spring (Type II); (b) Compression spring (Type IV).

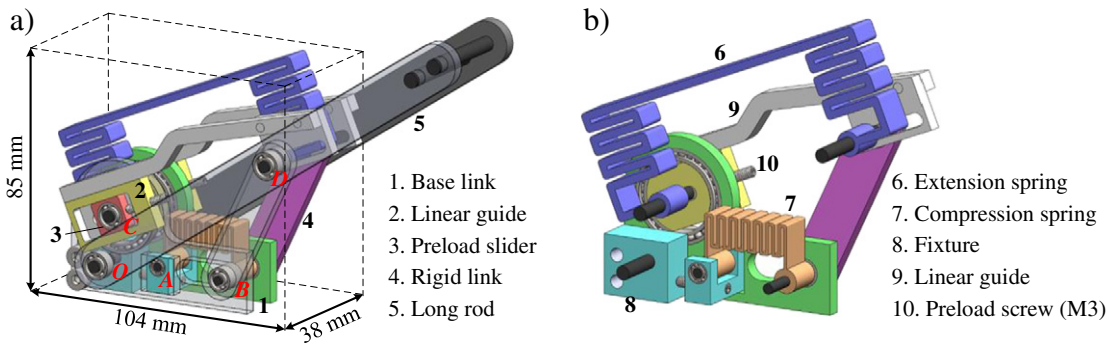

Fig. 19. (a) CAD model of the GBM; (b) Interior view of the GBM.

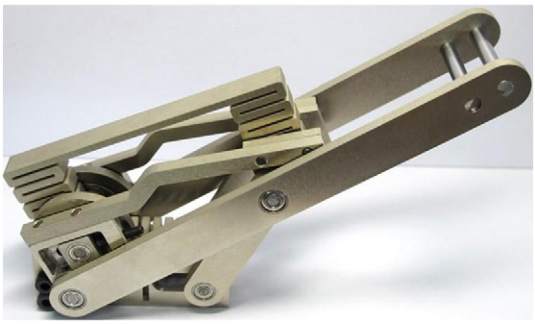

Fig. 20. Photo of the GBM prototype.

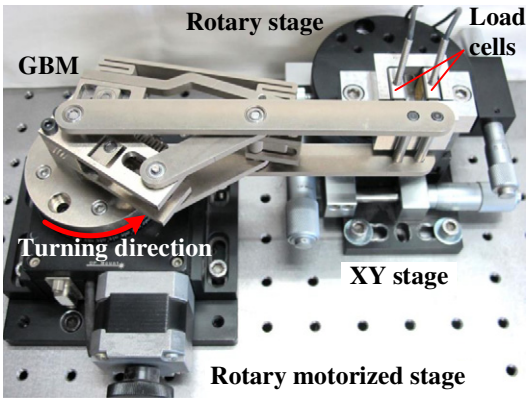

Fig. 21. Experimental setup.

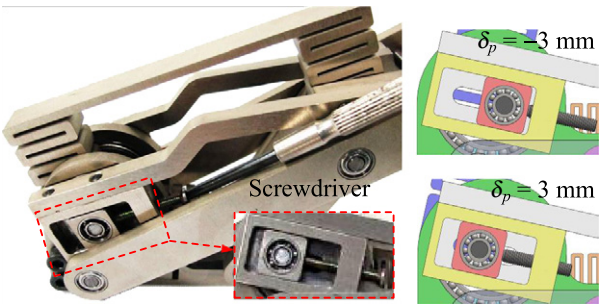

Fig. 22. Preload adjustment using a screwdriver.

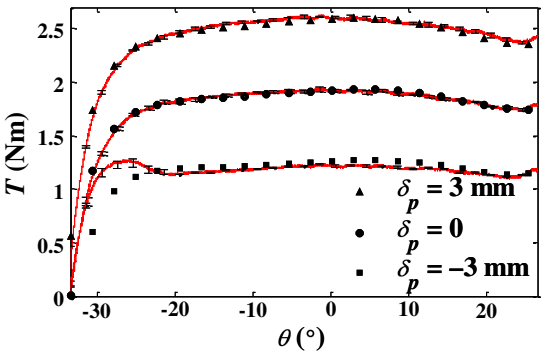

Fig. 23. Experimental torque curves (marks are simulation results).

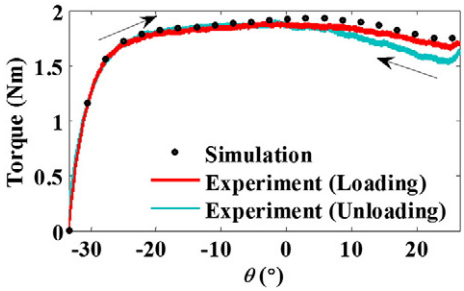

Fig. 24. Loading and unloading curves of $\delta_p = 0$.

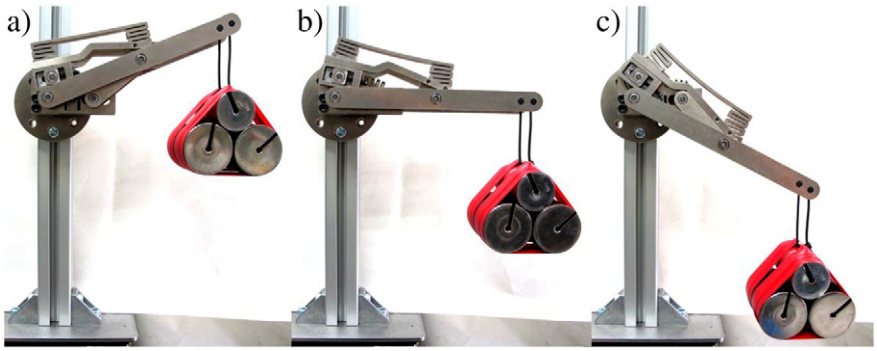

Fig. 25. Photo of payload balancing: (a) $\theta = -23°$; (b) $\theta = 0°$; (c) $\theta = 26°$.

Fig. 23. Each experiment was repeated three times in order to obtain the error bars. The triangular, circular, and square marks were the respective simulation results. As can be seen, the experimental curves matched the simulation ones quite well. For the curve of, $\delta_p = -3$ mm, there was a slight overshoot between $\theta = -33°$ and $-25°$. During this region, the preload slider moved to the right to contact with the preload screw. This contact produced a sudden force increase for the extension spring and thus the overshoot. This slight overshoot only occurred at large negative preload and did not affect the main balancing range. In the balancing range, the maximum error was less than 0.05 Nm. Fig. 24 further shows the loading and unloading curves of $\delta_p = 0$. From $\theta = 10°$ to 26°, there was a difference (maximum 0.15 Nm) between the two curves. This difference was mainly caused by the friction force at the revolute joints, especially in the unloading direction. If a friction coefficient of 0.02 is used for all the revolute joints, the simulated maximum torque curve gap between the loading and unloading directions would be nearly 0.15 Nm (at $\theta = 26°$), which matches with the difference measured by experiment. Fig. 25 illustrates the GBM for balancing an actual payload of 1.30 kg. The three subfigures denote the output link at $\theta = -23°$, 0°, and 26°, respectively. The payload could be moved almost freely in the balancing range.

Compared with the GBMs in Fig. 1(b)–(e), the proposed GBM has the following advantages.

1. The proposed GBM mainly consists of revolute joints. There are no pulley–cable pairs or cam–follower pairs that would be more vulnerable to wear and fatigue under repeated use. The springs in the GBM do not need to emulate the condition of zero initial length. Hence the number of components can be reduced.
2. The rotating components of the GBM are concentrated in the vicinity of the base joint *O*. No springs or wires would protrude out of the mechanism. This kind of design can avoid interference with the environment.
3. The proposed design uses two linear springs rather than one. Unlike previous GBMs that require the change of spring stiffness or spring attachment point, the proposed GBM depends on spring preload to adapt to different payloads. The amount of preload is very small and thus requires no extra space. The preload adjustment can be easily achieved through screws. The balancing range is the same for all adjustments.

6. Conclusions

This paper has presented a novel GBM to gravity-balance a single degree-of-freedom manipulator. The GBM requires two linear springs: one extension spring and one compression spring. The force of the extension spring needs to be transmitted to produce a nearly linear torque curve with slight stiffness variation. The force of the compression spring needs to be transmitted to produce a bistable torque curve. The two curves are combined to generate the required nonlinear torque curve. A special planar spring design has been proposed to accommodate the two springs in the same plane without causing interference. The sizes of the springs have been minimized so that the GBM is compact and have no components that are susceptible to wear and fatigue. A scaling rule for

the GBM is provided so that it can be applied to different payloads. Using simple screws to preload the extension spring, the GBM can be adjusted on-line to meet a different balancing capacity. The torque–displacement curves have been demonstrated through prototype experiments. We expect that the proposed mechanism can be used for applications that require gravity balancing.

Acknowledgments

This research project was supported by Ministry of Science and Technology of Taiwan, through Grant No. MOST103-2221-E-006-038.

References

[1] M. Kolarski, M. Vukobratović, B. Borovac, Dynamic analysis of balanced robot mechanisms, Mech. Mach. Theory 29 (3) (1994) 427–454.
[2] T. Laliberté, C.M. Gosselin, M. Jean, Static balancing of 3-DOF planar parallel mechanisms, IEEE/ASME Trans. Mechatron. 4 (4) (1999) 363–377.
[3] V. Arakelian, S. Ghazaryan, Improvement of balancing accuracy of robotic systems: application to leg orthosis for rehabilitation devices, Mech. Mach. Theory 43 (5) (2008) 565–575.
[4] S.K. Agrawal, Abbas Fattah, Gravity-balancing of spatial robotic manipulators, Mech. Mach. Theory 39 (12) (2004) 1331–1344.
[5] S. Shirata, A. Konno, M. Uchiyama, Design and evaluation of a gravity compensation mechanism for a humanoid robot, IEEE/RSJ International Conference on Intelligent Robots and Systems 2007, pp. 3635–3640.
[6] H.S. Kim, J.B. Song, Low-cost robot arm with 3-DOF counterbalance mechanism, IEEE International Conference on Robotics and Automation 2013, pp. 4183–4188.
[7] T. Rahman, R. Ramanathan, R. Seliktar, W. Harwin, A simple technique to passively gravity-balance articulated mechanisms, J. Mech. Des. 117 (4) (1995) 655–658.
[8] N. Schmit, M. Okada, Optimal design of nonlinear springs in robot mechanism: simultaneous design of trajectory and spring force profiles, Adv. Robot. 27 (1) (2013) 33–46.
[9] W.D. van Dorsser, R. Barents, B.M. Wisse, M. Schenk, J.L. Herder, Energy-free adjustment of gravity equilibrators by adjusting the spring stiffness, Proc. Inst. Mech. Eng. C J. Mech. Eng. Sci. 222 (9) (2008) 1839–1846.
[10] R. Barents, M. Schenk, W.D. van Dorsser, B.M. Wisse, J.L. Herder, Spring-to-spring balancing as energy-free adjustment method in gravity equilibrators, ASME J. Mech. Des. 133 (2011) 061010.
[11] M.J. French, M.B. Widden, The spring-and-lever balancing mechanism, George Carwardine and the Anglepoise lamp, Proc. Inst. Mech. Eng. C J. Mech. Eng. Sci. 214 (3) (2000) 501–508.
[12] G.W. Brown, "Equipment for use with hand held motion picture cameras", U.S. Patent No. 4,017,168. 12 Apr. 1977.
[13] A.H. Stienen, E.E. Hekman, G.B. Prange, M.J. Jannink, F.C. van der Helm, H. van der Kooij, Freebal: design of a dedicated weight-support system for upper-extremity rehabilitation, J. Med. Devices 3 (4) (2009) 041009.
[14] P.Y. Lin, W.B. Shieh, D.Z. Chen, A theoretical study of weight-balanced mechanisms for design of spring assistive mobile arm support (MAS), Mech. Mach. Theory 61 (156–167) (2013) 2013.
[15] S.K. Agrawal, S.K. Banala, A. Fattah, V. Sangwan, V. Krishnamoorthy, J.P. Scholz, W.-L. Hsu, Assessment of motion of a swing leg and gait rehabilitation with a gravity balancing exoskeleton, IEEE Trans. Neural Syst. Rehabil. Eng. 15 (3) (2007) 410–420.
[16] T. Rahman, et al., Passive exoskeletons for assisting limb movement, J. Rehabil. Res. Dev. 43 (5) (2006) 583–590.
[17] Y.-H. Chen, C.-C. Lan, An adjustable constant-force mechanism for adaptive end-effector operations, ASME J. Mech. Des. 134 (2012) 031005.
[18] Y.-S. Wu, C.-C. Lan, Linear variable-stiffness mechanisms based on preloaded curved beams, ASME J. Mech. Des. 136 (12) (2014) 122302.
[19] C.-C. Lan, Y.-J. Cheng, Distributed shape optimization of compliant mechanisms using intrinsic functions, ASME J. Mech. Des. 130 (7) (2008) 072304.
[20] C.-C. Lan, K.-M. Lee, Generalized shooting method for analyzing compliant mechanisms with curved members, ASME J. Mech. Des. 128 (4) (2006) 765–775.